Discrete Huygens' Metasurface: Realizing Anomalous Refraction and Diffraction Mode Circulation with a Robust, Broadband and Simple Design

Chu Qi and Alex M. H. Wong

***Abstract*—Metasurfaces composed of subwavelength unit cells usually require a large number of unit cells which leads to complicated design and optimization. Aggressive discretization in metasurface designs can significantly reduce the number of unit cells within a period, resulting in large unit cell sizes. The enlarged unit cells will encounter negligible mutual couplings when combined together, hence making straightforward the process of metasurface design. These advantages combine to allow the design of a novel class of metasurfaces which support the high efficiency redirection of electromagnetic (EM) waves over a wide bandwidth and operation angle. Moreover, an aggressively discretized metasurface can realize diffraction mode circulation. In this work we propose a simple transmissive metasurface which can realize diffraction mode circulation by refracting plane waves from angles of $-45°$, $0°$, $45°$ to angles of $0°$, $45°$, $-45°$ respectively. The power efficiency of each anomalous refraction is more than 80% at the design frequency of 28 GHz, and the 3-dB power efficiency bandwidth is 11%. We fabricated and measured the metasurface, the experiment results agree well with the simulation results.**

***Index Terms*—Discrete metasurface, Huygens' metasurface, anomalous refraction, mode circulation.**

I. Introduction

Metasurfaces are artificial surfaces with subwavelength-thickness which can break the limitation of natural surfaces and provide versatile control of electromagnetic (EM) waves [1]-[5]. In recent years, Huygens' metasurfaces have attracted increasing attention because of their simultaneous electric and magnetic responses to an incident EM wave [6]-[11]. The general design procedure for a Huygens' metasurface is to first design a continuous function of surface impedance (or admittance) which satisfies the boundary condition of the given incident and the desired reflected and/or transmitted EM waves. Then the metasurface is finely discretized into small elements, each of which realizes the sampled values of surface impedance at their respective locations. This is done by designing the unit cells with different geometrical structures and/or parameters. Finally, the elements are fitted together to form the composite metasurface. It is assumed that when the metasurface elements are sufficiently small, the composite metasurface will behave similarly to a surface whose surface impedance continuously varies in space. The detailed design process is described, for some examples, in [6], [7], [9], [12]-[14]. For a finely discretized metasurface design, the unit cell size is electrically small (typically about one-tenth of a wavelength), which sometimes results in fabrication difficulty. The small unit cells often lead to significant mutual coupling among the unit cells, which can affect the performance of the metasurface. To mitigate the effect of mutual coupling, the final design often requires further optimization, which complicates the design process. Meanwhile, many different unit cells are needed to achieve the different surface impedances, some surface impedance values may require strongly resonant metasurface element designs, the usage of which will compromise the robustness and bandwidth of the metasurface.

More recently, researchers have proposed the concept of the metagrating, which is a metasurface where each period is designed as a single scatterer, without further discretization [15]. The period of a metagrating controls the number of propagating modes. In the case of reflection with only two propagating diffraction modes (upon oblique incidence), with the specular mode suppressed, all the reflected power will couple to the desired mode, realizing high efficient anomalous reflection, sometimes with simplified structures [15]-[17]. However, more complicated designs are required to manage the diffraction of more propagating modes. Some researchers introduce more degrees of freedom with extra inclusions in each period, which complicates the theory and structure, as the mutual couplings among the inclusions are difficult to rigorously analyze [15], [18]-[20]. Some researchers use iterative optimization methods to design metagratings based on multimode geometrical structures, which need a lot of simulation iterations, and the optimized performance may differ depending on the specific application and the optimization algorithm [21], [22].

In parallel, our group has presented the aggressively discretized metasurface, which is designed to have as few elements as possible within a period, and can realize efficient control of propagating diffraction modes [23]-[25]. Different from metagratings which treat and design the metasurface period as a single entity, in a discretized metasurface design, we adopt the procedure of discretizing the metasurface period and design each element separately. The discretization level is chosen from spectral domain considerations, and thereafter, through an inherently discrete formulation, we directly solve for the required properties of the discretized elements. Aggressive discretization in metasurface design can dramatically reduce the number of elements and significantly enlarge the size of the elements, which leads to simplicity and robust performance.

In this work, we propose an aggressively discretized metasurface with three elements per period, which can realize efficient anomalous refraction by deflecting a normal incidence to 45°. Curiously, due to the aggressive discretization, the metasurface can also efficiently refract incident waves from –45° and 45° to angles of 0° and –45° respectively, hence achieving mode circulation. For each anomalous refraction case, our proposed metasurface can realize a power efficiency of higher than 80% at the design frequency of 28 GHz, and a 3-dB power efficiency bandwidth of 11%.

The rest of this communication is organized as follows. Section II introduces the metasurface discretization and design formulation. Section III details our simulation setup and results. Section IV describes our fabrication and experimental results. We discuss salient points of our work in Section V and conclude in Section VI.

II. Metasurface Discretization and Design Formulation

In this section, we will introduce the theoretical analysis and design formulation of a discretized periodic metasurface. After that, we propose an example to realize anomalous refraction with an aggressively discretized metasurface. Additionally, we investigate the mode circulation effect in the discretized metasurface designs.

A. *k*-space Operation of a Periodic Metasurface

We find it instructive to investigate the discretization of a periodic metasurface by examining the waveform contents in the frequency domain (*k*-space). Fig. 1(a) shows the *k*-space operation of a periodic metasurface. When a periodic metasurface is illuminated by a plane wave in free space, the output (i.e. the transmitted and/or reflected

This work was supported by an Early Career Scheme from the Research Grants Council of the Hong Kong under Grant 21211619 (*Corresponding author: Alex M. H. Wong*).

The authors are with the State Key Laboratory of Terahertz and Millimeter Waves, Department of Electrical Engineering, City University of Hong Kong, Hong Kong (e-mail: chuqi2-c@my.cityu.edu.hk; alex.mh.wong@cityu.edu.hk).

This article has been accepted for publication in a future issue of this journal, but has not been fully edited. Content may change prior to final publication. Citation information: DOI 10.1109/TAP.2022.3164931, IEEE Transactions on Antennas and Propagation

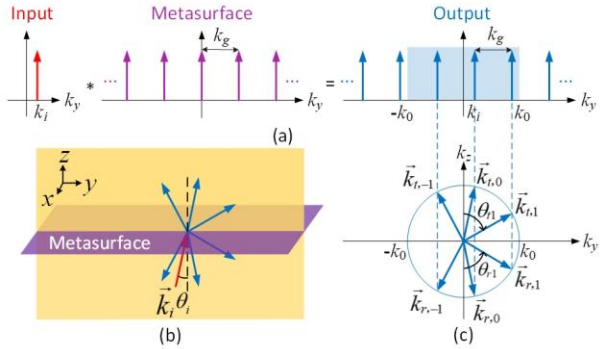

Fig. 1. (a) k-space operation of a periodic metasurface which varies along y-direction. The asterisk sign ($*$) denotes the convolution operation. Arrows indicate the existence of diffraction modes with different tangential wave numbers. The blue box in the output k-space spectrum denotes the propagation range of $k_y \in [-k_0, k_0]$. (b) A schematic diagram of a transmissive metasurface upon an incidence with wave number $\vec{k}_i$ and incident angle θ_i. (c) A schematic of output spectrum, $\vec{k}_{t,n}$ and $\vec{k}_{r,n}$ (n = –1, 0, 1) are the wave numbers of the n^{th}diffraction modes in the transmission and reflection region respectively.

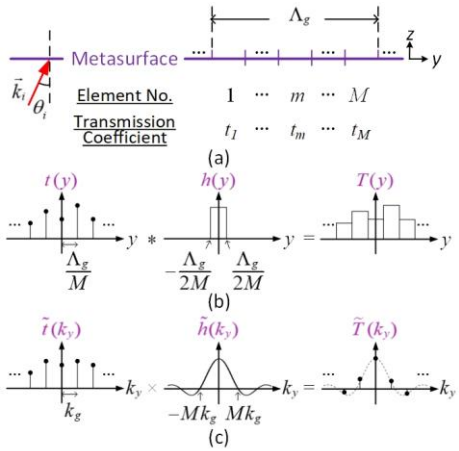

Fig. 2. (a) Schematic of one period of a transmissive metasurface with a discretization level of M elements per period. (b) Wave transmission through the metasurface in the spatial (y) domain. (c) Wave transmission through the metasurface in the tangential wave number (k_y) domain. The asterisk sign ($*$) denotes the convolution operation and the multiplication sign ($\times$) denotes the multiplication operation.

wave) will consist of an infinite number of diffraction modes. The tangential wave number of the n^{th} diffraction mode in the output k-space spectrum is

$$k_n = k_i + nk_g, \tag{1}$$

where

$$k_i = k_0 \sin\theta_i \text{ and } k_g = 2\pi/\Lambda_g. \tag{2}$$

Here k_i is the tangential wave number of the incident plane wave with incident angle θ_i, k_0 is the free space wave number, k_g is the wave number of the metasurface with period Λ_g. Of the infinite number of diffraction modes, only the ones in the propagation range of $k_y \in [-k_0, k_0]$ can scatter into the far field, and the ones out of the propagation range are evanescent. Fig. 1(b) is a schematic diagram of a transmissive metasurface in Fig. 1(a). For a transmissive metasurface, there is a same number of propagating diffraction modes in the transmission and reflection spectrum respectively. Fig. 1(c) is a schematic of the reflected and transmitted waves, corresponding to the output spectrum shown in Fig. 1(a). The refraction/reflection angles can be determined using

$$\theta_{t,n} = \theta_{r,n} = \sin^{-1}(k_n/k_0). \tag{3}$$

While the incident angle (θ_i) and metasurface period (Λ_g) determine the tangential wave numbers of the diffraction modes (k_n) in the output spectrum, the structure of the metasurface and its interaction with the incident EM wave will determine the magnitude and phase of each diffraction mode. That is, by engineering the transmission and/or reflection characteristics of the discretized metasurface elements, we can engineer the excitation of the transmission and/or reflection diffraction modes. In the following, we describe a way to calculate the required transmission coefficients for a discrete set of metasurface elements, which will transform a known incident wave into a desired set of transmitted plane waves.

B. Discretized Metasurface – Design Formulation

An aggressively discretized metasurface can be treated as an array of similar-sized and shaped scatterers which have similar scattering patterns. Therefore, we use array theory to investigate the scattering of a periodic metasurface.

Consider a transmissive metasurface illuminated by a plane wave with a tangential wave number k_i, travelling in the +z direction and encountering a metasurface at z = 0. The transmitted electric field at $z = 0^+$ is:

$$E_t(y) = T(y)E_i e^{-jk_i y}, \tag{4}$$

where E_i is a constant representing the complex amplitude of the incident electric field and $T(y)$ is the transmission function of the metasurface along the variation direction (y-direction). Fig. 2(a) shows a schematic of a metasurface with period Λ_g and a discretization level of M elements per period: each element has a size of Λ_g/M in the variation direction, the m^{th} element has a transmission coefficient of t_m, which can be written as

$$t_m = |t_m| e^{j\varphi_m}, \tag{5}$$

where $|t_m|$ and φ_m are the magnitude and phase of the transmission coefficient associated with the element. Figs. 2(b) and (c) show the transmission of the periodic metasurface in the spatial (y) domain and the tangential wave number (k_y) domain respectively. As shown in Fig. 2(b), $T(y)$ is the transmission function of the discretized metasurface, where $t(y)$ and $h(y)$ are the array function and element function of the transmission coefficients respectively. That is

$$T(y) = t(y) * h(y), \tag{6}$$

where $t(y) = \sum_m t[y_m]\delta(y - y_m)$, $t[y_m]$ is the transmission coefficient of the element located at y_m. Defining $\tilde{t}(k_y)$, $\tilde{h}(k_y)$ and $\tilde{T}(k_y)$ as the Fourier transform pairs of $t(y)$, $h(y)$ and $T(y)$ respectively, we have

$$\tilde{T}(k_y) = \tilde{t}(k_y) \times \tilde{h}(k_y). \tag{7}$$

From Fourier transform theory, $\tilde{T}(k_y)$ can be written as a summation of delta functions where each delta function corresponds to a diffraction mode in the transmission spectrum, i.e., $\tilde{T}(k_y) = \sum_n \tilde{T}[k_{y,n}]\delta(k_y - k_{y,n})$. Since $t[y_m]$ is discrete with spacing Λ_g/M between adjacent elements and periodic of M elements, Fourier transform theory guarantees that, $\tilde{t}[k_{y,n}]$ will be discrete with interval $k_g = 2\pi/\Lambda_g$ between adjacent modes and periodic of M modes. Using $t[m]$ and $\tilde{t}[n]$ to denote the m^{th} and n^{th} items in $t[y_m]$ and $\tilde{t}[k_{y,n}]$ respectively, we have

$$t[m] = \sum_{n=1}^{M} \tilde{t}[n] e^{jn\frac{2\pi}{M}m}, \tilde{t}[n] = \frac{1}{M}\sum_{m=1}^{M} t[m] e^{-jn\frac{2\pi}{M}m}, \tag{8}$$

which is to say, $t[m]$ and $\tilde{t}[n]$ are Fourier series pairs. Here we consider the element function $h(y)$ as a rectangular function, which means we

This article has been accepted for publication in a future issue of this journal, but has not been fully edited. Content may change prior to final publication. Citation information: DOI 10.1109/TAP.2022.3164931, IEEE Transactions on Antennas and Propagation

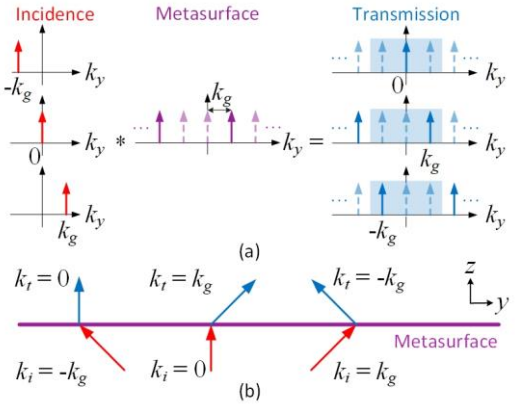

Fig. 3. (a) The *k*-space operation of a metasurface featuring the circulation of three diffraction modes. Arrows with solid line represent diffraction modes with non-zero magnitude, while arrows with dashed line represent diffraction modes with zero magnitude. (b) A schematic diagram of the transmissive metasurface in (a).

assume wave-transmission homogeneity within each element. Therefore, we have

$$h(y)=\begin{cases}1, & -\frac{\Lambda_g}{2M}<y<\frac{\Lambda_g}{2M}\\ 0, & otherwise.\end{cases},\ \tilde{h}(k_y)=\frac{2\pi}{Mk_g}\mathrm{sinc}\left(\frac{k_y}{Mk_g}\right). \quad (9)$$

The n^{th} item of $\tilde{T}[k_{y,n}]$, which we denote as $\tilde{T}[n]$, corresponds to the coefficient of the $-n^{\text{th}}$ diffraction mode in the transmission spectrum. That is, we can find the coefficient of the n^{th} diffraction mode, a_n, using (8) – (9):

$$\begin{aligned}a_n &= E_i\tilde{T}[-n]=E_i\tilde{t}[-n]\times\tilde{h}(-nk_g)\\ &=\frac{E_i\Lambda_g}{M^2}\mathrm{sinc}\left(-\frac{n}{M}\right)\sum_{m=1}^{M}t[m]e^{jn\frac{2\pi}{M}m}.\end{aligned} \quad (10)$$

Therefore, with a given discretization level (M) and transmission coefficient of each element ($|t_m|$ and φ_m for $m=1,\cdots,M$), we can calculate the magnitude ($|a_n|$) and phase ($\angle a_n$) of each diffraction mode in the transmission spectrum.

While the preceding formulation *analyzes* the diffraction modes excited by a given incident wave and metasurface, we now present a formulation to find the required transmission coefficients which *synthesize* a desired transmission spectrum. Writing (10) in matrix form, we have

$$\vec{a}=C_0D\vec{t}, \quad (11)$$

where

$$\vec{a}=\begin{bmatrix}\vdots\\ a_{-1}\\ a_0\\ a_1\\ \vdots\end{bmatrix}_{N\times1},\ \vec{t}=\begin{bmatrix}t_1\\ \vdots\\ t_M\end{bmatrix}_{M\times1},\ C_0=\frac{E_i\Lambda_g}{M^2},$$

$$D=\begin{bmatrix}\vdots & \vdots & \vdots\\ \mathrm{sinc}\left(\frac{-1}{M}\right)e^{-j2\pi\frac{1}{M}} & \dots & \mathrm{sinc}\left(\frac{-1}{M}\right)e^{-j2\pi\frac{M}{M}}\\ 1 & \dots & 1\\ \mathrm{sinc}\left(\frac{1}{M}\right)e^{j2\pi\frac{1}{M}} & \dots & \mathrm{sinc}\left(\frac{1}{M}\right)e^{j2\pi\frac{M}{M}}\\ \vdots & \vdots & \vdots\end{bmatrix}_{N\times M}. \quad (12)$$

$\vec{a}$ is an *N*-element vector composed of the coefficients of the diffraction modes which need to be controlled. When $M\geq N$, (11) – (12) can be solved to find the required elements' transmission coefficients ($\vec{t}$) for a given transmission spectrum ($\vec{a}$). When $M=N$, the solution is unique. That is, to realize control of *N* diffraction modes, the lowest number of elements required (the most aggressive discretization level) is $M=N$.

C. Anomalous Refraction Metasurface Design

We now use the aforementioned method to design an aggressively discretized metasurface which realizes anomalous refraction by deflecting a normal incidence to 45°. Applying (1) – (3), one can see that the anomalous refraction can be realized by a metasurface with $k_g=k_0\sin45°=k_0/\sqrt{2}$. This metasurface has three propagating diffraction modes, the –1st, 0th and 1st diffraction modes, among which only the 1st diffraction mode ($k_1=k_g$) has non-zero magnitude. According to the design formulation, the three propagating diffraction modes can be controlled with an aggressive discretization level of $M=3$. Therefore, we can solve for the three elements' transmission coefficients using (11) – (12) with the condition $[a_{-1},a_0,a_1]=[0,0,1]$. The resultant transmission coefficient, normalized to the first term, is $[1,e^{-j2\pi/3},e^{j2\pi/3}]$. In other words, the three elements should have uniform transmission magnitudes and equidistant transmission phases. Fig. 3 (middle panel) shows the *k*-space operation and the refraction property of this metasurface.

We now implement the discrete *elements* with metasurface *unit cells*. In an earlier work [25] we have applied a discrete formulation similar to Section II B to discretize the metasurface in [6] into 3 elements, then simulated an implementation with 3 identical unit cells per element (i.e. 9 unit cells per period, compared to 20 unit cells per period in [6]). In [25] we show that this discretization results in an enlargement of unit cells along with a slight performance improvement. In the present paper, we further enlarge the unit cell size by implementing each element with just a single unit cell (i.e. 3 unit cells per period). We shall show, by simulation and experiment, that such a highly discretized design achieves excellent anomalous refraction despite a vast reduction in the number of unit cells per period. Such a reduction increases the minimum feature size, which simplifies metasurface fabrication.

While the complex transmission coefficients obtained here can also be obtained by sampling a gradient phase profile with $M=3$, our discrete formulation makes several unique contributions. Firstly, it shows that the employed level of discretization suffices to perform anomalous refraction with, in theory, perfect efficiency, given the availability of elements possessing the required transmission coefficients. The same can not be guaranteed by a metasurface designed with a continuous phase/impedance profile but implemented with a coarse sampling of the profile. Secondly, our design formulation can be applied to realize functionalities where the corresponding output spectra consist of multiple diffraction modes. Thirdly, our design formulation includes all diffraction modes excited by the incident wave, including both propagating and evanescent modes. Information on these modes helps us to realize the mode circulation effect, which we will discuss in detail in the next subsection.

D. The Mode Circulation Effect

Due to aggressive discretization in the spatial domain, the metasurface attains a periodic behavior in *k*-space which leads to an intriguing phenomenon which we term the mode circulation effect. We elucidate this effect from the *k*-space perspective introduced above. Fig. 3(a) shows the *k*-space operation for the metasurface designed in the previous subsection. For the metasurface, we show the -2nd to 2nd diffraction modes as they can map into the propagation range upon the appropriate incidence plane waves. The other diffraction orders contribute to evanescent waves regardless of the wave incidence direction. As depicted, the diffraction amplitudes are $[a_{-2},a_{-1},a_0,a_1,a_2]=[a_{-2},0,0,a_1,0]:\{a_{-1},a_0,a_1\}$ are prescribed in metasurface design while $a_{-2}\neq0$ and $a_2=0$ are obtained from periodic repetition, noting that the metasurface has a repetition level of $M=3$. For this metasurface, upon plane wave incidence at $k_{i,-1}=-k_g\Rightarrow\theta_{i,-1}=-45°$ (top panel of Fig. 3(a)), the only non-zero diffraction mode within the propagation range in the transmission *k*-space spectrum is $k_{t,1}=k_{i,-1}+k_g=0$. Similarly, upon incidence with $k_{i,0}=0$, $\theta_{i,0}=0°$ (middle panel of Fig. 3(a)), the only non-zero propagating mode in the transmission spectrum is $k_{t,1}=k_{i,0}+k_g=k_g$. However, upon incidence with $k_{i,1}=k_g$ and $\theta_{i,1}=45°$ (bottom panel of

This article has been accepted for publication in a future issue of this journal, but has not been fully edited. Content may change prior to final publication. Citation information: DOI 10.1109/TAP.2022.3164931, IEEE Transactions on Antennas and Propagation

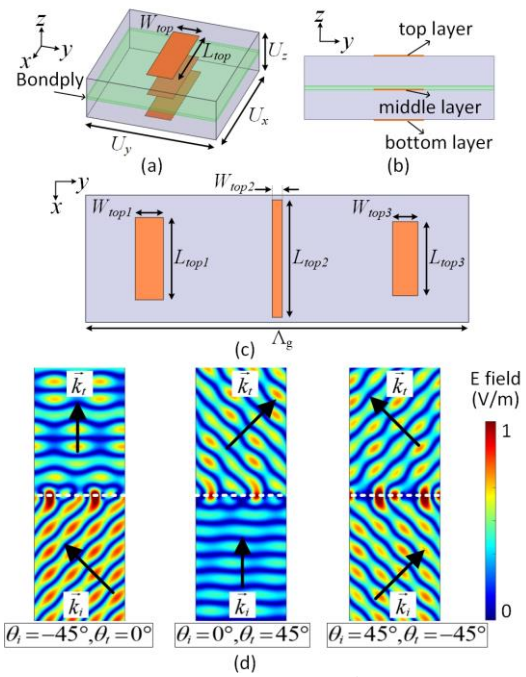

Fig. 4. (a) Perspective view and (b) Front view of the geometrical structure of the unit cell. The size of the unit cell is $U_x = U_y = 5$ mm, $U_z = 1.67$ mm. (c) Top view of one period of the proposed metasurface. (d) The electric field magnitude distributions of the metasurface upon incident plane waves with incident angles of –45°, 0° and 45° respectively.

Fig. 3(a)), the only non-zero propagating mode in the transmission spectrum is $k_{t,-2} = k_{i,1} - 2k_g = -k_g$. Summarizing these relationships, we see that this metasurface can realize the circulation of three diffraction modes by turning the -1st, 0th, +1st diffraction orders into the 0th, +1st, -1st diffraction orders respectively. In terms of plane wave angles, the metasurface refracts waves from $\theta_i = \{-45°, 0°, 45°\}$ to $\theta_t = \{0°, 45°, -45°\}$ respectively, as shown in Fig. 3(b).

The mode circulation effect exemplifies intriguing phenomena that can readily be explained by a discrete formulation of metasurface design, but are highly unobvious under a continuous formulation. Further, the nature of mode circulation is directly affected by the discretization level: the mode circulation characteristics will change with the discretization level, and may become altogether unobservable in the limit of fine discretization, unless careful consideration is also given based on the *k*-space operation. Hence the discrete metasurface design formulation hereby proposed provides additional handles to complement existing methods mostly based on continuous metasurface boundaries, and can serve as a valuable tool for metasurface analysis and design.

In summary, we have theoretically shown, based on the metasurface discretization and design formulation, that a periodic metasurface can realize efficient anomalous refraction of a normal incidence with an aggressive discretization level of three elements per period. Additionally, the aggressive discretization can lead to mode circulation effect. In the following sections, we will report simulation and experimental results showing the realization of anomalous refraction and mode circulation by a discrete metasurface with high efficiency and broadband performance.

III. Metasurface Design and Simulation

In this section, we report the design of a transmissive discrete Huygens' metasurface, as an example to show that a discrete metasurface can achieve anomalous refraction and mode circulation with high efficiency. We design the metasurface at 28 GHz. Using (2) with $k_g = k_0 \sin 45°$, we find the metasurface period $\Lambda_g = 15$ mm. The aggressively discretized metasurface has three elements per period. We design each element as one unit cell. Ansys HFSS is used for the simulation. Figs. 4(a) and (b) show the geometrical structure of the unit cell, which is constructed using three layers of rectangular patches. Here we adopted the bianisotropic Huygens' metasurface unit cell structure, which is proven to provide great flexibility to synthesize perfect anomalous refraction boundaries [9], [12], [13]. As the unit cell is large compared to most surfaces, we find we can employ simple metallic patterns on each layer and still achieve efficient anomalous refraction for our purpose.

The metasurface is designed on two Rogers RT/duroid 5880 boards (ε_r= 2.2, δ_t= 0.0009) with a substrate thickness of 0.787 mm and copper cladding thickness of 17.8 μm (1/2 oz.). They are bonded by a bondply (Rogers RO 4450F, ε_r = 3.52, δ_t = 0.004) with a thickness of 0.1 mm. The electric field is along *x*-axis. By sweeping the dimensions of the rectangular patches on each layer, we can get the transmission coefficients of the unit cell with different geometrical parameters. We choose three unit cells with similar transmission magnitudes (around 0.9) and equidistant transmission phases (120°) to compose the period of the metasurface, as was found necessary in Section II C. The enlarged unit cell size and simple structure result in negligible couplings among unit cells along the variation direction (*y*-direction). Thus, we directly combine the chosen unit cells to form the metasurface, no optimization is performed afterward. Fig. 4(c) shows a period of the metasurface; Table I details the geometrical parameters. 2D periodic simulation shows that this metasurface can refract incident waves with incident angles of –45°, 0° and 45° to transmitted waves with refracted angles of 0°, 45° and –45° with power efficiencies of 81.3%, 81.8% and 80.1% respectively. The simulated 3-dB power efficiency bandwidth of this metasurface is 11%. Fig. 4(d) shows the electric field magnitude distributions of the metasurface upon incident plane waves with incident angles of –45°, 0° and 45° respectively. From these full-wave simulation results we can see that the designed metasurface achieves anomalous refraction and mode circulation with high efficiency at the design frequency.

TABLE I

Geometrical Parameters of the Unit Cells

Unit cell No.	L_{top} [mm]	W_{top} [mm]	L_{mid} [mm]	W_{mid} [mm]	L_{bot} [mm]	W_{bot} [mm]
1	3.2	1.1	3.0	1.3	3.4	0.9
2	4.6	0.4	2.6	0.6	4.7	0.6
3	2.9	1.0	2.4	1.0	2.9	1.0

IV. Fabrication and Experiment

We proceed to fabricate and measure the proposed metasurface. Fig. 5(a) shows a photo of the fabricated metasurface. The size of the fabricated metasurface is 195×195 mm^2. Figs. 5(b) and (c) show one period of our proposed metasurface compared with a transmissive Huygens' metasurface proposed in [6], which can realize anomalous refraction by deflecting a normal incidence by 30°. We observe that, compared to finely discretized metasurface design, the aggressively discretized metasurface can lead to much larger unit cells and benefit from a very simple design, which relaxes fabrication tolerances. A more detailed comparison is presented in the discussion section.

Fig. 6(a) shows a schematic of the experimental setup. In the setup, the transmitting antenna (a 4-40 GHz double ridged horn NSI-RF-RGP-40) is fixed with the metasurface with incident angles of –45°, 0° and 45° respectively, for the three refraction cases. The receiving antenna (an 18-40 GHz standard diagonal horn FR-6413) rotates to measure the scattering of the metasurface at the transmission side. Fig. 6(b) shows a photo of the experimental setup. In the experiment, the metasurface is embedded into a metallic board to eliminate direct transmission between the transmitting and receiving horns. Fig. 6(c) compares the measured and simulated anomalous refraction power efficiencies. The measured power efficiency is the ratio between the power received in the desired refraction direction and the power illuminated onto the metasurface. At the design frequency of 28 GHz,

This article has been accepted for publication in a future issue of this journal, but has not been fully edited. Content may change prior to final publication. Citation information: DOI 10.1109/TAP.2022.3164931, IEEE Transactions on Antennas and Propagation

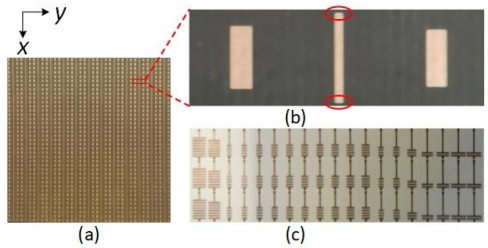

Fig. 5. (a) The fabricated metasurface. (b) One period of our proposed metasurface compared with (c) one period of the metasurface proposed in [6].

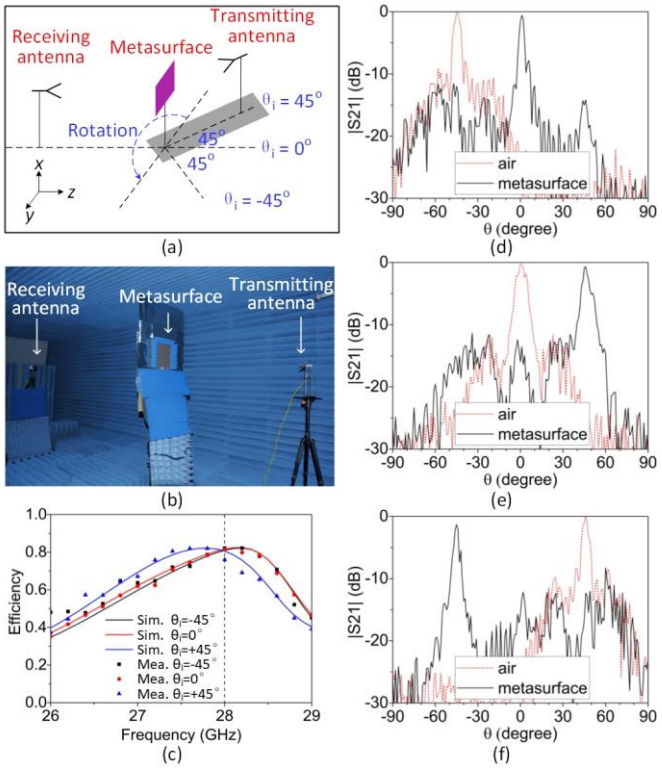

Fig. 6. Experiment. (a) A schematic of experimental setup. (b) A photo of the experimental setup. (c) The measured and simulated anomalous refraction power efficiencies. (d) – (f) Measured scattering of the metasurface compared with the scattering of air (same setup without metasurface) upon incidences of –45°, 0° and 45° respectively.

the measured power efficiencies of the fabricated metasurface are 82.2%, 81.6% and 76.0% for anomalous transmission cases of incidences from –45°, 0° and 45° to refracted directions of 0°, 45° and –45° respectively. Besides, the efficiency performance over the 3-dB frequency band agrees well with the simulated result. Figs. 6(d), (e) and (f) show, at the design frequency, the measured scattering of the metasurface compared with the scattering of air under incident angles of –45°, 0° and 45° respectively. As we can see, the metasurface can efficiently refract plane waves with incident angles of –45°, 0° and 45° to refracted waves with refraction angles of 0°, 45° and –45° respectively, realizing diffraction mode circulation. In all the three cases, sidelobe levels are lower than –10 dB, showing that the metasurface achieves a strong suppression of spurious scattering along with high-efficiency anomalous transmission to the desired modes.

V. Discussion

A. Feature Size Comparison

In discrete metasurface design, the enlarged unit cell size and simple structure can greatly relax the fabrication tolerance, which

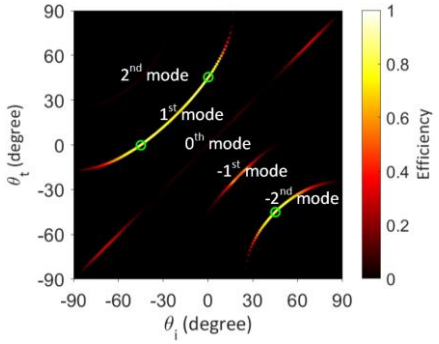

Fig. 7. Transmission of the proposed metasurface as a function of the incident angle. Incidences with angles of –45°, 0°, 45° are marked with green circles.

will benefit the metasurface design at high frequencies and even optical frequencies. To show this, we compare our proposed metasurface with a finely discretized transmissive Huygens' metasurface proposed in [6]. The structures of the fabricated metasurfaces are shown in Figs. 5(b) and (c), one period is shown for both metasurfaces. With an aggressively discretized metasurface design, we can dramatically increase the unit cell size without compromising on the anomalous refraction performance. This allows us to relax the critical feature size. The minimum feature size in our design is $0.03\lambda_0$, which is about 6-fold increased from the design in [6]. (We use the electrical length here to compare metasurfaces which are built for different frequencies of operation.) In our design, the smallest gap (0.3 mm) is easily fabricable by conventional etching technology. Extension to even higher frequencies (up to 100 GHz) should be straightforward. We attempt to further increase the minimum feature size by removing the two smallest gaps. The smallest gap on the top layer is circled in Fig. 6(b); a gap of a similar dimension also exists in the bottom layer. The resultant structure, after the removal of the gaps, boosts a minimum feature size of $0.15\lambda_0$, while the simulated anomalous refraction efficiency slightly reduces to 70%. This amended metasurface has a similar anomalous refraction efficiency as [6], but a minimum feature size which is 28-fold increased. Despite the relaxed feature size, our proposed metasurface produces at a larger refraction angle and operates with higher anomalous refraction power efficiency. Similar feature size improvements are observed in comparison to more recent works on bianisotropic Huygens' metasurfaces, but a quantitative comparison is not performed with these works since the refraction angles are drastically different. In summary, the aggressive discretization in a metasurface design can lead to simple structures with large feature sizes, without sacrificing the metasurface efficiency. This can prove useful for practical and high-frequency applications.

B. Anomalous Refraction for Other Incident Angles

While we have concentrated on the metasurface's performance at $\theta_i = \{-45°, 0°, 45°\}$, it can also realize efficient anomalous refraction upon other angles of incidence. Fig. 7 shows wave transmission through the metasurface as a function of the incident angle θ_i, as obtained from simulation with material losses included. The operation points for the mode circulation are denoted with circles. As predicted by the k-space operation, for $-k_0 < k_i < k_0 - k_g$ (–90°<θ_i<17°), the 1st diffraction mode is dominant. For $2k_g - k_0 < k_i < k_0$ (24.5°<θ_i<90°), the –2nd diffraction mode is dominant. For $k_0 - k_g < k_i < 2k_g - k_0$ (17°<θ_i<24.5°), the behavior is less well-defined, as the propagating modes are designed to propagate weakly, and the unit cells are designed to reflect weakly. As a result, slight deviations from the required element properties will appreciably affect the scattering of the metasurface. In this case an appreciable refraction, mainly to the –1st diffraction mode, is

observed. We further observe that, when $\{\theta_i, \theta_t\}$ fall within [–60°, +60°], and when there exists a propagation mode to which the incident power is directed (in our case either the –2nd or 1st diffraction mode), the power efficiency is more than 70%, showcasing the respectable efficiency of the metasurface over a wide angular range.

C. *Effects of Spatial Dispersion*

In the design formulation, we assume that the element function $h(y)$ is invariant with k_i, i.e., $h(y)$ remains the same for different incident angles. In practice the metasurface unit cell may be spatially dispersive, but in our case such a spatial dispersion effect is minor because the element size ($0.47\lambda_0$) is small compared to the wavelength, and the incident angles are within a relatively small range ($\leq 45°$). Fig. 7 has shown that our proposed design, without adaptation from spatial dispersion considerations, performs anomalous refraction with respectable efficiency for angles within ±60°. For an improved performance at a large angle, one can account for spatial dispersion by using the accurate unit cell scattering pattern $\tilde{h}(k_y)$ corresponding to the desired angle of incidence, as obtained from a full-wave simulation.

VI. Conclusion

We have shown, theoretically and experimentally, that aggressive discretization can benefit a metasurface design with simplicity and good performance. The aggressive discretization in metasurface design leads to a dramatically reduced number of elements with a much larger element size. This allows us to achieve efficient EM wave manipulation using a metasurface with a very simple structure that relaxes fabrication tolerances. This in turn allows one to avoid the use of unit cells with compromised properties or with strong resonance, resulting in efficient and broadband performance. Moreover, the aggressive discretization in metasurface design can provide control handles to facilitate diffraction mode circulation. Here we designed and fabricated a discrete transmissive Huygens' metasurface with a simple structure – it features rectangular microstrip patterns, with the critical feature size 28-fold increased compared with a finely-discretized anomalous refraction Huygens' metasurface. It can realize efficient anomalous refraction by deflecting a normal incidence to 45°. Meanwhile, due to its aggressively discretized design, the proposed metasurface can also realize efficient refraction of plane waves from –45° and 45° to 0° and –45° respectively, thus realizing diffraction mode circulation. Our proposed metasurface has a good performance with more than 80% power efficiency and 11% 3-dB power efficiency bandwidth. The aggressive discretization can benefit the metasurface design at high frequencies and even optical frequencies. The concept of using a discrete metasurface to realize mode circulation effect can also be applied to guided waves and multi-channel communication systems.

References

[1] C. L. Holloway, E. F. Kuester, J. A. Gordon, J. O'Hara, J. Booth, and D. R. Smith, "An overview of the theory and applications of metasurfaces: The two-dimensional equivalents of metamaterials," *IEEE Antennas Propag. Mag.*, vol. 54, no. 2, pp. 10–35, 2012.

[2] N. Yu, P. Genevet, M. A. Kats, F. Aieta, J.-P. Tetienne, F. Capasso, and Z. Gaburro, "Light propagation with phase discontinuities: Generalized laws of reflection and refraction," *Science*, vol. 334, no. 6054, pp. 333–337, 2011.

[3] S. B. Glybovski, S. A. Tretyakov, P. A. Belov, Y. S. Kivshar, and C. R. Simovski, "Metasurfaces: From microwaves to visible," *Phys. Rep.*, vol. 634, pp. 1–72, 2016.

[4] N. M. Estakhri and A. Alu, "Wave-front transformation with gradient metasurfaces," *Phys. Rev. X*, vol. 6, no. 4, p. 041008, 2016.

[5] C. Pfeiffer and A. Grbic, "Bianisotropic metasurfaces for optimal polarization control: Analysis and synthesis," *Phys. Rev. Appl.*, vol. 2, no. 4, p. 044011, 2014.

[6] J. P. S. Wong, M. Selvanayagam, and G. V. Eleftheriades, "Design of unit cells and demonstration of methods for synthesizing Huygens metasurfaces," *Photonics Nanostruct*, vol. 12, no. 4, pp. 360–375, 2014.

[7] A. Epstein and G. V. Eleftheriades, "Huygens' metasurfaces via the equivalence principle: Design and applications," *J. Opt. Soc. Am. B*, vol. 33, no. 2, pp. A31–A50, 2016.

[8] F. S. Cuesta, I. A. Faniayeu, V. S. Asadchy, and S. A. Tretyakov, "Planar broadband Huygens' metasurfaces for wave manipulations," *IEEE Trans. Antennas Propag.*, vol. 66, no. 12, pp. 7117–7127, 2018.

[9] M. Chen, E. Abdo-Sanchez, A. Epstein, and G. V. Eleftheriades, "Theory, design, and experimental verification of a reflectionless bianisotropic Huygens' metasurface for wide-angle refraction," *Phys. Rev. B*, vol. 97, no. 12, p. 125433, 2018.

[10] A. M. H. Wong and G. V. Eleftheriades, "Active Huygens' box: Arbitrary electromagnetic wave generation with an electronically controlled metasurface," *IEEE Trans. Antennas Propag.*, vol. 69, no. 3, pp. 1455–1468, 2021.

[11] A. Epstein, J. P. S. Wong, and G. V. Eleftheriades, "Cavity-excited Huygens' metasurface antennas for near-unity aperture illumination efficiency from arbitrarily large apertures," *Nat. Commun.*, vol. 7, no. 1, pp. 1–10, 2016.

[12] A. Epstein and G. V. Eleftheriades, "Arbitrary power-conserving field transformations with passive lossless omega-type bianisotropic metasurfaces," *IEEE Trans. Antennas Propag.*, vol. 64, no. 9, pp. 3880–3895, 2016.

[13] M. Chen and G. V. Eleftheriades, "Omega-bianisotropic wire-loop Huygens' metasurface for reflectionless wide-angle refraction," *IEEE Trans. Antennas Propag.*, vol. 68, no. 3, pp. 1477–1490, 2019.

[14] M. Chen, A. Epstein, and G. V. Eleftheriades, "Design and experimental verification of a passive Huygens' metasurface lens for gain enhancement of frequency-scanning slotted-waveguide antennas," *IEEE Trans. Antennas Propag.*, vol. 67, no. 7, pp. 4678–4692, 2019.

[15] Y. Ra'di, D. L. Sounas, and A. Alu, "Metagratings: Beyond the limits of graded metasurfaces for wave front control," *Phys. Rev. Lett.*, vol. 119, no. 6, p. 067404, 2017.

[16] O. Rabinovich and A. Epstein, "Analytical design of printed circuit board (pcb) metagratings for perfect anomalous reflection," *IEEE Trans Antennas Propag.*, vol. 66, no. 8, pp. 4086–4095, 2018.

[17] O. Rabinovich, I. Kaplon, J. Reis, and A. Epstein, "Experimental demonstration and in-depth investigation of analytically designed anomalous reflection metagratings," *Phys. Rev. B*, vol. 99, no. 12, p. 125101, 2019.

[18] O. Rabinovich and A. Epstein, "Arbitrary diffraction engineering with multilayered multielement metagratings," *IEEE Trans. Antennas Propag.*, vol. 68, no. 3, pp. 1553–1568, 2019.

[19] Z. Zhang, M. Kang, X. Zhang, X. Feng, Y. Xu, X. Chen, H. Zhang, Q. Xu, Z. Tian, W. Zhang *et al.*, "Coherent perfect diffraction in metagratings," *Adv. Mater.*, vol. 32, no. 36, p. 2002341, 2020.

[20] A. Casolaro, A. Toscano, A. Alu, and F. Bilotti, "Dynamic beam steering with reconfigurable metagratings," *IEEE Trans. Antennas Propag.*, vol. 68, no. 3, pp. 1542–1552, 2019.

[21] J. Jiang, D. Sell, S. Hoyer, J. Hickey, J. Yang, and J. A. Fan, "Free-form diffractive metagrating design based on generative adversarial networks," *ACS Nano*, vol. 13, no. 8, pp. 8872–8878, 2019.

[22] D. Sell, J. Yang, S. Doshay, R. Yang, and J. A. Fan, "Large-angle, multifunctional metagratings based on freeform multimode geometries," *Nano Lett.*, vol. 17, no. 6, pp. 3752–3757, 2017.

[23] A. M. H. Wong, P. Christian, and G. V. Eleftheriades, "Binary Huygens' metasurfaces: Experimental demonstration of simple and efficient neargrazing retroreflectors for TE and TM polarizations," *IEEE Trans. Antennas Propag.*, vol. 66, no. 6, pp. 2892–2903, 2018.

[24] A. M. H. Wong and G. V. Eleftheriades, "Perfect anomalous reflection with a bipartite Huygens' metasurface," *Phys. Rev. X*, vol. 8, no. 1, p. 011036, 2018.

[25] C. Qi and A. M. H. Wong, "A coarsely discretized Huygens' metasurface for anomalous transmission," in *2019 IEEE Asia-Pacific Microwave Conference (APMC)*. IEEE, 2019, pp. 935–937.

[26] G. Lavigne, K. Achouri, V. S. Asadchy, S. A. Tretyakov, and C. Caloz, "Susceptibility derivation and experimental demonstration of refracting metasurfaces without spurious diffraction," *IEEE Trans. Antennas Propag.*, vol. 66, no. 3, pp. 1321–1330, 2018.